ACS APPLIED MATERIALS & INTERFACES

Research Article

Cite This: ACS Appl. Mater. Interfaces 2019, 11, 3809−3822

www.acsami.org

Laser-Activatable CuS Nanodots to Treat Multidrug-Resistant Bacteria and Release Copper Ion to Accelerate Healing of Infected Chronic Nonhealing Wounds

Yue Qiao,[†,‡,⋈] Yuan Ping,[∥,⋈] Hongbo Zhang,[#,⋈] Bo Zhou,[‡] Fengyong Liu,[∇] Yinhui Yu,[†,○] Tingting Xie,[‡] Wanli Li,[‡] Danni Zhong,[‡] Yuezhou Zhang,[#] Ke Yao,[†,○] Hélder A. Santos,*[,◆,¶] and Min Zhou*[,†,‡,§,⊥]

[†]Eye Center & Department of Nuclear Medicine, The Second Affiliated Hospital, Zhejiang University School of Medicine, Hangzhou 310009, China

[‡]Institute of Translational Medicine and [§]Key Laboratory of Cancer Prevention and Intervention, National Ministry of Education, Zhejiang University, Hangzhou 310009, China

[∥]College of Pharmaceutical Sciences and [⊥]State Key Laboratory of Modern Optical Instrumentations, Zhejiang University, Hangzhou 310058, China

[#]Department of Pharmaceutical Science Laboratory, Åbo Akademi University, Turku 20520, Finland

[∇]Department of Interventional Radiology, Chinese PLA General Hospital, Beijing 100853, China

[○]Zhejiang Provincial Key Laboratory of Ophthalmology, Hangzhou 310009, China

[◆]Drug Research Program, Division of Pharmaceutical Chemistry and Technology, Faculty of Pharmacy and [¶]Helsinki Institute of Life Science, HiLIFE, University of Helsinki, Helsinki FI-00014, Finland

Supporting Information

ABSTRACT: Chronic nonhealing wounds have imposed serious challenges in the clinical practice, especially for the patients infected with multidrug-resistant microbes. Herein, we developed an ultrasmall copper sulfide (covellite) nanodots (CuS NDs) based dual functional nanosystem to cure multidrug-resistant bacteria-infected chronic nonhealing wound. The nanosystem could eradicate multidrug-resistant bacteria and expedite wound healing simultaneously owing to the photothermal effect and remote control of copper-ion release. The antibacterial results indicated that the combination treatment of photothermal CuS NDs with photothermal effect initiated a strong antibacterial effect for drug-resistant pathogens including methicillin-resistant *Staphylococcus aureus* (MRSA) and extended-spectrum β-lactamase *Escherichia coli* both in vitro and in vivo. Meanwhile, the released Cu^{2+} could promote fibroblast cell migration and endothelial cell angiogenesis, thus accelerating wound-healing effects. In MRSA-infected diabetic mice model, the nanosystem exhibited synergistic wound healing effect of infectious wounds in vivo and demonstrated negligible toxicity and nonspecific damage to major organs. The combination of ultrasmall CuS NDs with photothermal therapy displayed enhanced therapeutic efficacy for chronic nonhealing wound in multidrug-resistant bacterial infections, which may represent a promising class of antibacterial strategy for clinical translation.

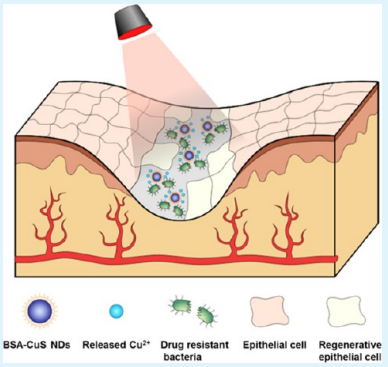

KEYWORDS: *antibacterial effect, multidrug-resistant bacteria, chronic nonhealing wound, copper sulfide nanodots, photothermal effects*

1. INTRODUCTION

One of the complications associated with patients diagnosed with diabetes mellitus is chronic wound infection.[1,2] Due to the nonhealing nature of chronic diabetes wounds, their bacterial infection is becoming a major challenge for both treatments and management in the clinical practice.[3−5] For example, diabetic patients with foot ulcers often suffer from bacterial infection, thereby increasing the risk of morbidity and mortality.[6] Antibiotic therapies for chronic diabetic wounds are often futile, largely due to the formation of the extracellular polymeric substances (biofilms).[7,8] These biofilms are generated during the growth of bacteria, which may prevent antibiotics from penetrating into wound beds. Up to now, there are limited reports of effective therapeutic approaches for alleviating the symptom of chronic wound infection, or accelerating the wound-healing process. Thus, development of alternative therapeutic modalities is essential to address the current challenges.

Received: December 15, 2018
Accepted: January 3, 2019
Published: January 3, 2019

DOI: 10.1021/acsami.8b21766
ACS Appl. Mater. Interfaces 2019, 11, 3809−3822

Copper ions are essential catalysts of many enzymes, proteins, and transcription factors, including vascular endothelial growth factors (VEGF), nerve growth factors, matrix metalloproteinases, glycyl-L-histidyl-L-lysine tripeptide, etc., to properly maintain the function.[9] They play an important role in many wound-healing processes and serve as antiseptic and antimicrobial agents. Copper ions are also reported to possess hypoxia-mimicking capacities, which facilitate the stabilization of hypoxia-induced factors (HIFs) to promote upregulation of the downstream-targeted genes, including VEGF, thereby enhancing angiogenesis.[10−12] In addition, as one of the most important trace elements for human beings, copper ions can enhance bone density by inhibiting active bone resorption. As a result, delivery of copper ions to the wound lesion is likely to improve antibacterial effects and promote wound healing.[13−17]

Recent studies indicated that nanomaterials with photothermal capabilities may serve as a new class of therapeutic agents for antibacterial therapy.[18−25] By virtue of their photothermal property, these materials converted heat energy from absorbed light energy to provide a robust approach to ablate infected bacteria. For example, the delivery of CuS nanoparticles (NPs) to the tumor tissue would allow for the photothermal therapy (PTT) through hyperthermia effect when the tumor was exposed to irradiation of near-infrared (NIR) laser.[26−32] Recent studies also indicated that CuS-based photothermal therapy (PTT) is a promising antiseptic strategy to combat antibacterial infection.[33−36] One intriguing feature is that the photothermal effect of CuS provides a robust and reversible strategy to directly ablate bacteria simply through the remote control of light irradiation, which minimizes the potential issues of antibiotic misuse. This inspires us to repurpose CuS-based NPs as the antibacterial agents for combating chronic wound infections.

In this study, we developed albumin-stabilized CuS nanoparticles as a powerful antibacterial agent to simultaneously exert antibacterial effect and accelerate wound-healing process. Specifically, the photothermal ability of CuS is exploited for ablating bacteria; the released Cu^{2+} is not only capable of promoting wound healing but also enhancing antibacterial effect. We demonstrated that such an antibacterial formulation is capable of eradicating multidrug-resistant (MDR) bacterial infection without damaging surrounding dermal tissues, and more importantly, accelerating wound-healing process of MDR bacteria-infected diabetic mice.

2. MATERIALS AND METHODS

2.1. Bacteria. Extended-spectrum β-lactamase *Escherichia coli* (ESBL, ATCC 35218), methicillin-resistant *Staphylococcus aureus* (MRSA, ATCC 43300), human foreskin fibroblast cell (HFF-1, ATCC SCRC-1041), and human umbilical vein endothelial cell (HUVEC, ATCC CRL-1730) were obtained from American Type Culture Collection (ATCC). BALB/c mice were obtained from Shanghai Bioscience Co., Ltd and diabetic mutant (db/db) mice were obtained from Changzhou Cavens Co., Ltd.

2.2. In Vitro Antibacterial Activity Analysis. Drug-resistant Gram-negative bacterial ESBL *E. coli* and MRSA were employed for the estimation of the synergistic antibacterial effects of CuS nanodots (NDs) plus NIR laser irradiation. Following activation and incubation, logarithmic growth phase bacterial was diluted 200-fold with fresh lysogeny broth (LB) medium and supplemented with different concentration series (2.81, 5.63, 11.25, 22.5, and 45.0 μg/mL) of CuS NDs and then illuminated with laser (808 nm, 2.5 W/cm^2) for 10 min. After shaking at 37 °C for 24 h, 100 μL bacterial suspension from each group was transferred into a sterile 96-well culture plate. Measurement of 600 nm wavelength optical absorbance (OD_{600}) by a microplate reader (SpectraMax M5) was taken, which indicated bacterial concentration for making a further calculation of survival rate. The bacterial suspensions were diluted 10^6-fold and then 100 μL of the bacterial dilutions was coated and incubated on LB agar plates with a spreader for overnight at 37 °C. Assessment of colony-forming unit (CFU) quantization was implemented by arithmetic on the basis of CFUs emergence. CuS NDs without laser and CuS NPs with/without laser were designed for control groups.

2.3. In Vivo Antibacterial Activity Analysis. All the experiments on animals were accredited by the institutional ethics committee and agreed with the requirements for the care and use of laboratory animals of Zhejiang University. Six-week-aged female BALB/c mice were obtained from Shanghai Slac Laboratory Animal Co., Ltd. The bacterial strain of MRSA was used for mouse infection in vivo model. Briefly, 4 groups of mice (n = 5/group) were anesthetized using 4% chloral hydrate (30 mg/kg) and then one wound hole was prepared on the backbone of the mouse with ophthalmic surgical scissors over a surface circle with a diameter of 0.7 cm. Afterward, 50 μL of MRSA suspension (2.0×10^7 CFU/mL) was used to infect the tissue of all the mice to establish an experimental model of infection. Twenty-four hours later, for the CuS NDs Laser group, CuS NDs (45 μg/mL, 50 μL) was smeared on the wounds, which were irradiated with an 808 nm laser (2.5 W/cm^2, 1 min), and the temperature changes of wounds were observed by thermographic pictures captured using infrared thermal imaging system. In the period of 12 days after the administration, the mice were monitored and wounds that were visually observed for recovery were measured by vernier caliper every 2 days. The CuS NDs, CuS NPs plus laser, and blank control groups were also carried out in the same procedure. Subsequently, the treated and control mice were euthanized under anesthesia by cervical dislocation and the infected tissue was excised to prepare pathological slides. For histological analysis, the tissue samples were soaked in 10% formalin solution, desiccated, paraffin embedded, and sectioned into 5 μm slices, which were then stained with hematoxylin and eosin (H&E). High-resolution images of all the histological slices were taken via virtual slide microscopy (Olympus VS120, Japan).

2.4. In Vitro Cell Migration. The HFF-1 cells were seeded in 24-well plates (10^4 cells per well) and allowed to form a confluent monolayer. After starvation with fetal bovine serum (FBS)-free medium for 24 h, the cell monolayer was scratched in a straight-line using a 200 μL pipette tip to mimic an incisional wound. Cells were then washed with phosphate-buffered saline to remove debris, treated with CuS NDs (45 μg/mL) upon laser irradiation (808 nm, 2.5 W/cm^2, 10 min), and incubated at 37 °C with the medium containing 1% FBS. Twenty-four hours later, the cells were photographed and cell migration rate was calculated. CuS NDs without laser irradiation, CuS NPs with laser irradiation and untreated group were designed as control.

2.5. In Vitro Cell Angiogenesis. The HUVECs (10^4 cells/well) were incubated in the treatment of CuS NDs (45 μg/mL) upon laser irradiation (808 nm, 2.5 W/cm^2, 10 min) with 1% FBS on Matrigel for 24 h at 37 °C. At each time point, the cells were photographed from three random fields on an inversion microscope. CuS NDs without laser irradiation, CuS NPs with laser irradiation, and untreated group were designed as control. The enclosed networks of complete tubes were digitally imaged and quantified using the Angiogenesis Analyzer plugin on ImageJ.

2.6. In Vivo Wound Healing Improvement Analysis. Diabetic mutant (db/db) mice (6 weeks aged, female) were operated to form MRSA infection wound model and treated with different therapies. The protocol was identical with that of in vivo antibacterial activity analysis excluding wounds area measurement interval time was 3 days and tissue slices were stained with Masson's trichrome (MT) staining after tissue fixation. Collagen tissue gap and thickness were quantized.

3. RESULTS AND DISCUSSION

3.1. Preparation and Characterization of CuS NDs. CuS NDs were synthesized by a facile single-step hydrothermal

DOI: 10.1021/acsami.8b21766
ACS Appl. Mater. Interfaces 2019, 11, 3809−3822

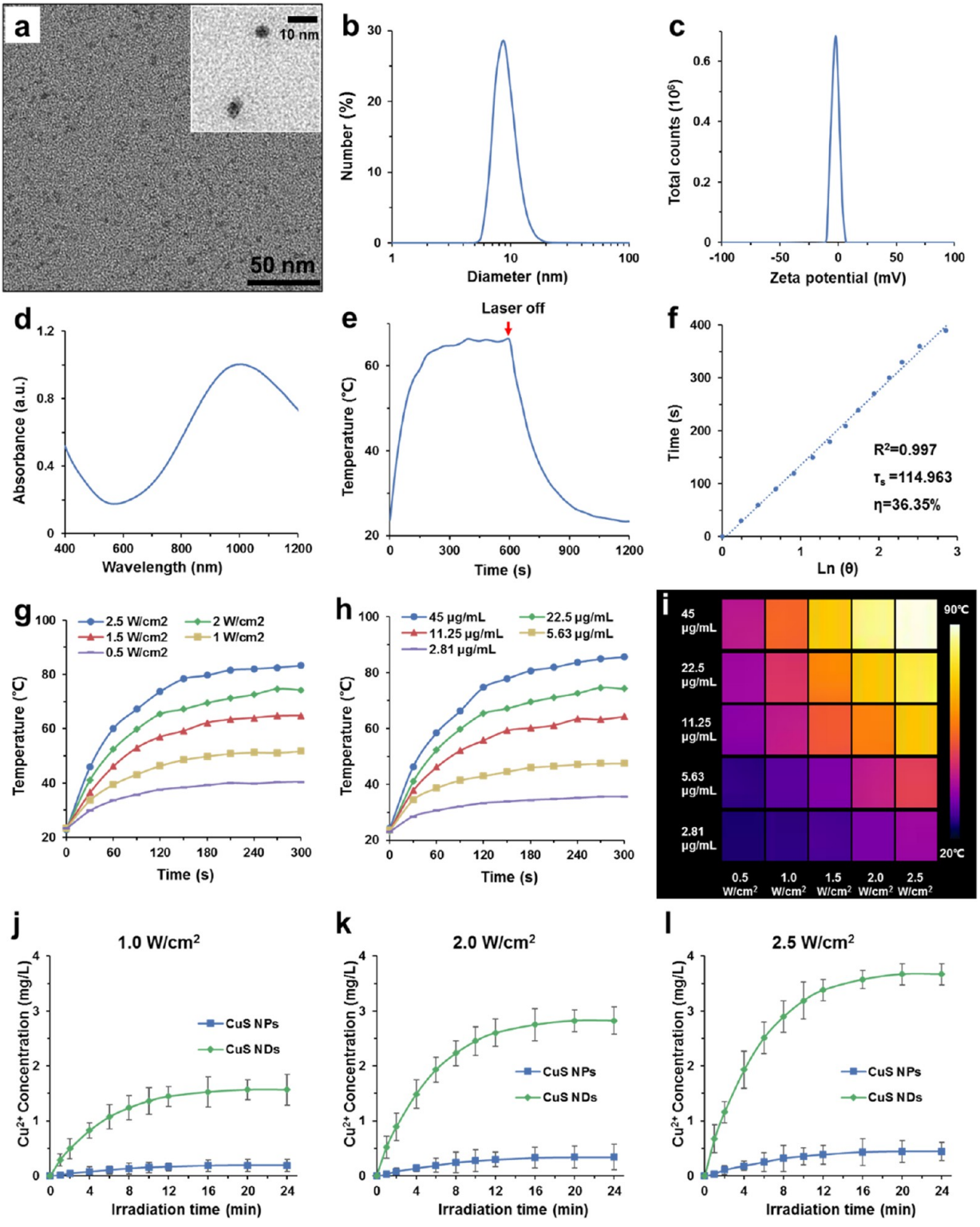

Figure 1. Characterization of CuS NDs. (a) TEM image of CuS NDs (inset: high-resolution TEM image). (b) Hydrodynamic diameter of CuS NDs measured by dynamic light scattering. (c) ζ-Potential of CuS NDs showing the surface charge is almost neutral. (d) UV−vis−NIR absorption spectrum of CuS NDs showing a strong absorbance band in the near-infrared region. (e) The temperature profiles of CuS NDs irradiated by NIR laser, followed by cooling down by turning off the laser light. An 808 nm laser with the power density of 1.5 W/cm^2 was used. (f) Linear time data versus $-\mathrm{Ln}(\theta)$ from the cooling period of panel versus negative natural logarithm of driving force temperature. (g) Temperature increment versus irradiation power density over a period of exposure to the 808 nm laser. The concentration of CuS NDs was 22.5 μg/mL. (h) Temperature increment over a period of exposure to the 808 nm laser (2.0 W/cm^2) at various CuS NDs concentrations. (i) The photothermal image array of CuS NDs photothermal performance versus different power densities and concentrations. (j–l) Cumulative amounts Cu^{2+} released from the CuS NDs or CuS NPs under irradiation over a period of exposure to the 808 nm laser with different laser power densities of (j) 1.0 W/cm^2, (k) 2.0 W/cm^2, and (l) 2.5 W/cm^2.

DOI: 10.1021/acsami.8b21766
ACS Appl. Mater. Interfaces 2019, 11, 3809−3822

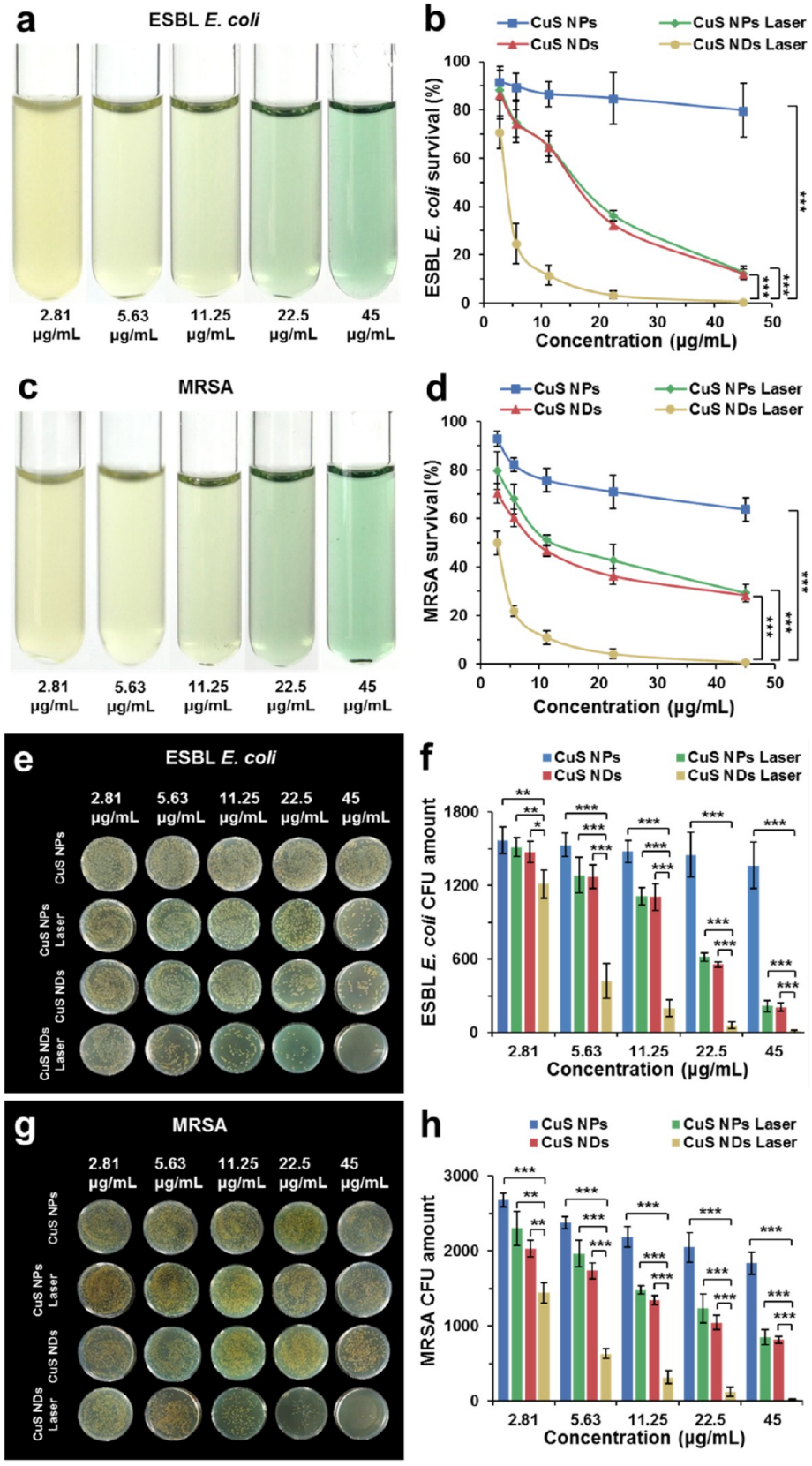

Figure 2. Antibacterial effect of CuS NDs PTT in vitro. Photographs and survival rates of ESBL *E. coli* (a, b) and MRSA *E. coli* (c, d) with various treatments at different NPs concentrations. Power density was 2.5 W/cm^2 for 10 min. (e, g) Photographs of ESBL *E. coli* and MRSA bacterial colonies formed on LB agar plates with various treatments at different concentrations. (f, h) The corresponding CFU count of ESBL *E. coli* and MRSA with various treatments. The power density was 2.5 W/cm^2 for 10 min (*p < 0.05, **p < 0.01, ***p < 0.001).

DOI: 10.1021/acsami.8b21766
ACS Appl. Mater. Interfaces 2019, 11, 3809−3822

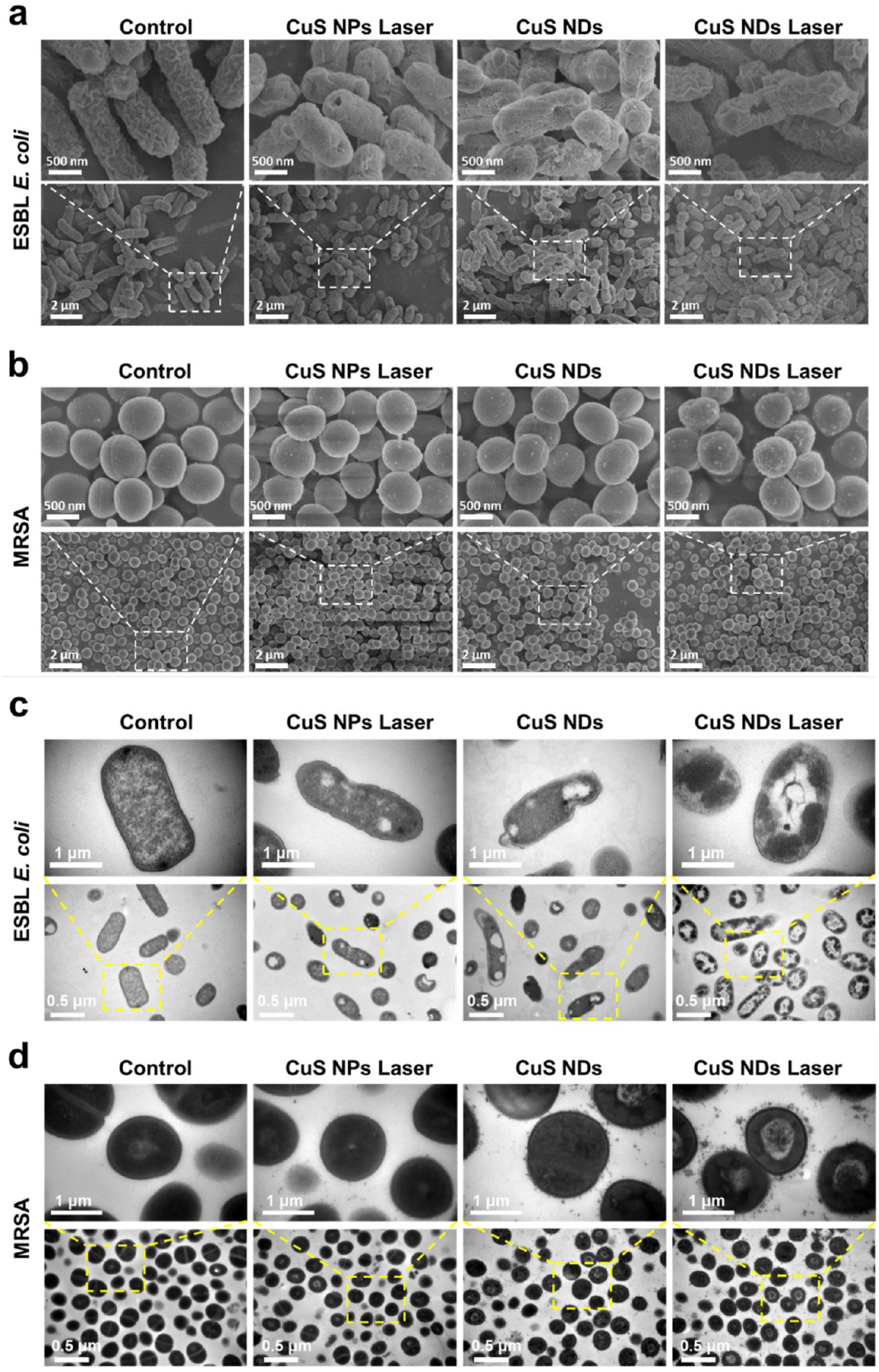

Figure 3. Bacteria's inner structure disruption and potential mechanism of CuS NDs PTT antibacterial effect. SEM images of (a) ESBL *E. coli* and (b) MRSA treated with different materials (45 μg/mL) upon laser irradiation (2.5 W/cm^2, 10 min). TEM images of (c) ESBL *E. coli* and (d) MRSA treated with different materials (45 μg/mL) upon laser irradiation (2.5 W/cm^2, 10 min).

route. Bovine serum albumin (BSA), a biocompatible and highly soluble protein, was used to control the particle size and stability during the preparation. A representative transmission electron microscopy (TEM) image (Figure 1a) demonstrated

DOI: 10.1021/acsami.8b21766
ACS Appl. Mater. Interfaces 2019, 11, 3809−3822

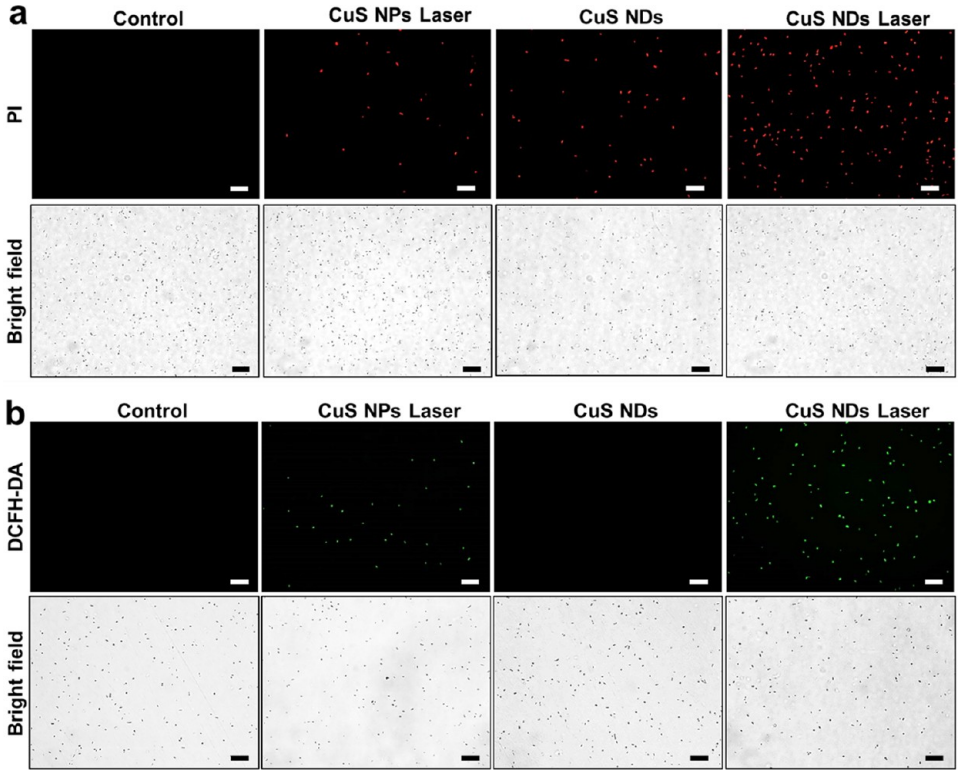

Figure 4. (a) Fluorescent and bright-field photographs of ESBL *E. coli* with different materials (45 μg/mL) upon laser irradiation (2.5 W/cm^2, 10 min), stained by PI following various treatments, bar = 50 μm. (b) In vitro ROS effects with various treatments. Fluorescent and bright-field photographs of ESBL *E. coli* with different materials (45 μg/mL) upon laser irradiation (2.5 W/cm^2, 10 min), stained by DCFH-DA, bar = 50 μm.

that the CuS NDs size was ca. 6 nm. The hydrodynamic diameter of CuS NDs (Figure 1b) was measured by dynamic light scattering analysis, and the average size (9 nm) was larger than those presented in TEM. The ζ-potential analysis of CuS NDs indicated a nearly neutral surface charge (−2.21 mV) (Figure 1c). Furthermore, the UV−NIR absorption spectrum showed a strong absorption band in the NIR window with a peak at 994 nm (Figure 1d), which may render the capability of CuS NDs for NIR-laser-induced photothermal conversion. We next systematically investigated the photothermal conversion efficiency of the CuS NDs. As shown in Figure 1e, the temperature of CuS NDs increased quickly within 5 min up to 65 °C and then reached a plateau. The photothermal conversion efficiency of CuS NDs was about 36.35% (Figure 1f), which was higher than that of many other known photothermal coupling agents and suggested a minimum injury to the surrounding normal tissues.

The temperature elevation was well correlated with laser power density and the concentration of nanoparticles (Figure 1g−i). It should be noted that when the concentration of CuS NDs was 22.5 μg/mL, the temperature of the solution was increased to ∼83.8 °C at 5 min with 2.5 W/cm^2 laser treatment, whereas only 40.5 °C was achieved under 0.5 W/cm^2 laser exposure. The data confirm that the excellent photothermal efficiency of CuS NDs could be achieved and tuned by adjusting the laser energy as well as the concentration of nanoparticles. PTT property of material was sometimes accompanied by photodynamic therapy (PDT) property and their several studies demonstrating CuS as a PDT agent.[29,37,38] To investigate the reactive oxygen species (ROS) level after the irradiation, we quantify the ROS level by measuring the fluorescence intensity from 2,7-dichlorofluorescein (DCF), which is converted by nonfluorescent 2,7-dichlorofluorescein diacetate (DCFH-DA) after ROS oxidization. As shown in Figure S1, fluorescence was hardly detected without laser irradiation, whereas both CuS NDs and CuS NPs group generate green fluorescence. CuS NDs showed stronger ROS generation capabilities as compared with CuS NPs, indicating their possible better antibacterial effect. Compared to the larger-sized CuS NPs (∼20 nm), the ultrasmall CuS NDs (∼6 nm) have a higher (∼36-folds) surface area and thus demonstrated a higher ROS signal due to the corresponding higher photodynamic conversion effects. The results demonstrate the comprehensive property of CuS NDs to synergistically kill bacteria by ROS generation and energy conversion.

3.2. Copper Ion (Cu^{2+}) Release under Laser Irradiation. Inspired by the ultrasmall size and the excellent NIR photothermal conversion effect of CuS NDs, we hypothesized that the synergistic effect could provide hyperthermia and stimulate Cu^{2+} release under the laser irradiation. Therefore, the amount of released Cu^{2+} in designed time points was analyzed from the solution of CuS NDs and CuS NPs undergo NIR laser irradiation. In experimental condition, the CuS NDs resulted in a distinctly high amount of Cu^{2+} release when the sample was irradiated for longer than 2 min compared with CuS NPs (Figure 1j−l), demonstrating the factor of ultrasmall size conductive to facilitate Cu^{2+} release from CuS particles in the laser irradiation condition. Cu^{2+} linearly released within the first 5 min and then gradually became constant. Notely, more Cu^{2+} was released when the sample was treated by higher laser power density, indicating their controllable release capability via the adjustable laser power density.

3.3. In Vitro Antibacterial Activity to Drug-Resistant Bacteria. The antibacterial activity of CuS NDs was

DOI: 10.1021/acsami.8b21766
ACS Appl. Mater. Interfaces 2019, 11, 3809−3822

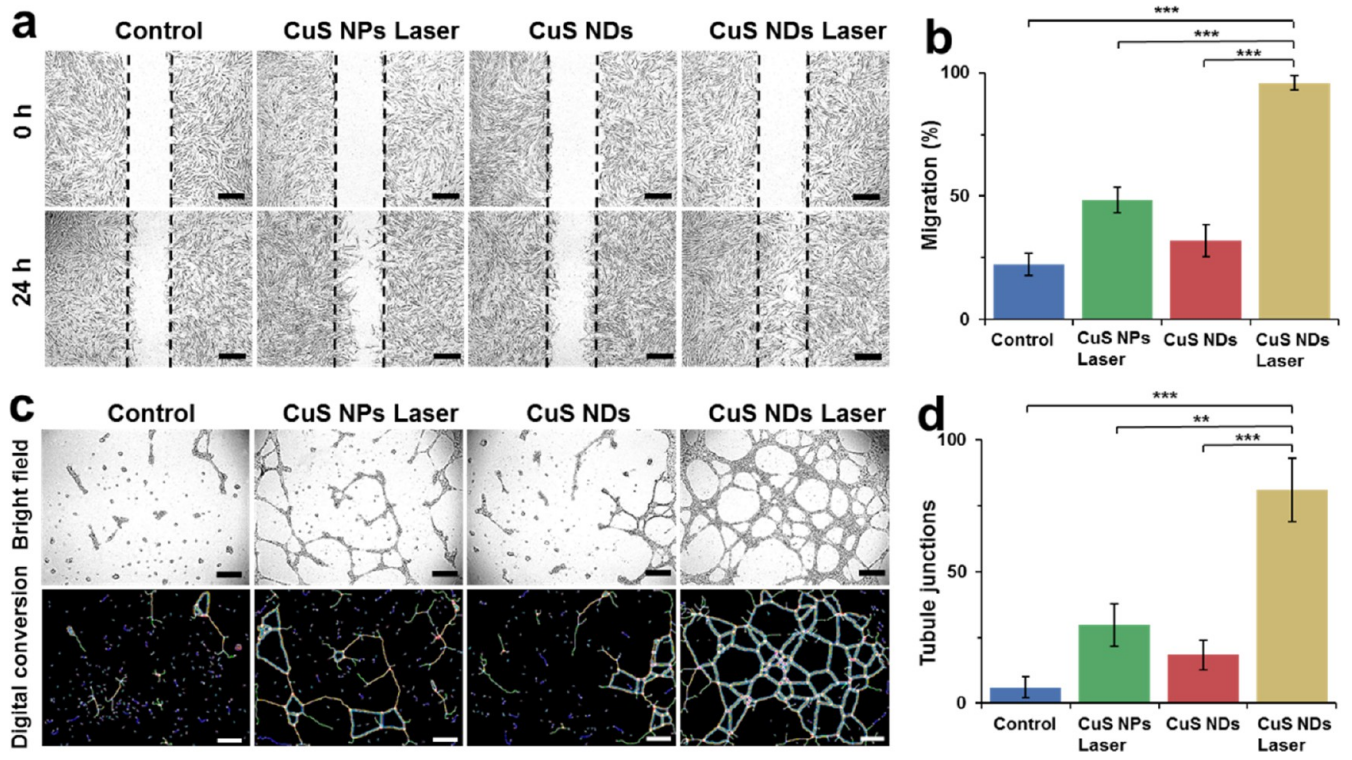

Figure 5. Promoting healing effects of and potential mechanism CuS NDs PTT in vitro/in vivo. (a) Digital images of Hiff-1 cells after treatment with CuS NPs laser, CuS NDs, and CuS NDs laser for 24 h, bar = 400 μm. (b) Quantification of HFF-1 cells migration. (c) Micrographs and digital analysis conversion of endothelial tubulogenesis of HUVECs based on the Matrigel in the presence of CuS NPs laser, CuS NDs, and CuS NDs laser for 24 h, bar = 400 μm. (d) Quantification of tubule junctions.

investigated using two drug-resistant bacterial strain models, namely, extended-spectrum β-lactamase-positive *E. coli* (ESBL *E. coli*) and methicillin-resistant *S. aureus* (MRSA). Turbidity, survival analysis, growth-inhibition assay, and spread plate method were applied in the experiment (Figure 2). In general, although CuS NPs exhibited a very weak antibacterial capacity against both strains, CuS NDs heavily inhibit the reproduction of both stains, as reflected by its dose-dependent assay. This is due to the enhanced water stability of CuS NDs, therefore, in favor of Cu^{2+} release compared to unstable CuS NPs in the suspension. When both formulations were exposed to laser irradiation, they all exhibited enhanced antibacterial effect, and CuS NDs could completely kill bacteria up to 45 μg/mL (CuS NDs). The CuS NDs plus laser irradiation treatment demonstrated much higher antibacterial effects than the CuS NPs plus irradiation treatment in both strains. These results were in accordance with the growth of bacteria (ESBL *E. coli* and MRSA) in Petri dishes after exposure to different treatments.

3.4. Evaluation of the Integrity of Bacteria. To further investigate the antibacterial mechanisms, cellular morphological changes of ESBL *E. coli* and MRSA following the treatment were studied via scanning electron microscopy (SEM). As demonstrated in Figure 3a, it was found that both bacteria without any treatment remained fully active with typical clubbed/spherical shape and intact smooth surface. In the case of ESBL *E. coli* treated with CuS NDs under NIR laser irradiation, their original morphology was distorted and displayed wrinkled bacterial cellular wall/membranes with clear lesions and hole. As to MRSA treated with CuS NDs under NIR laser irradiation (Figure 3b), a large amount of ultrasmall nanodots adhered to the bacterial surface were observed, which may be attributed to the strong interaction between CuS NDs and bacterial cellular wall. Using EDS element mapping technique, we also found amass of CuS NDs on the bacterial surface (Figure S2) when the bacteria was treated with CuS NDs plus laser.

TEM analysis showed that part of the outer membranes of the bacteria were damaged after CuS NPs plus laser or CuS NDs treatments. However, almost all of the bacterial membranes were lysed after CuS NDs plus laser treatments, leading to the loss of structural integrity of bacterial cell walls (Figure 3c). Also, the cytoplasm of the bacteria displayed aggregated obviously in both strains after CuS NDs plus laser irradiation, indicating the damage of the cells. There are many nanoparticles aggregation on the surface of the outer membrane after CuS NDs or CuS NDs plus laser treatment (Figure 3d), thus determining an enhanced permeability of the bacterial membrane, which allowed entry into the cell and, possibly, caused its death.

The bacteria survival rate was further verified by a fluorescence staining assay on the basis of the integrity of bacterial cellular wall/membrane.[25] As shown in Figure 4a, strongest red fluorescence could be observed in the group in which the bacteria were treated with CuS NDs with laser irradiation, indicating the strong antibacterial effect of CuS NDs after laser irradiation. Taken together, these results provided confirmative evidence that the strong interaction between CuS NDs and bacteria and photothermal effects from CuS NDs may be the key reason to induce the lysis of bacteria, which may influence intracellular metabolism to induce bacterial cell apoptosis.

3.5. ROS Effect and Photodynamic Therapy. In addition to above results, we further wish to explore whether

DOI: 10.1021/acsami.8b21766
ACS Appl. Mater. Interfaces 2019, 11, 3809−3822

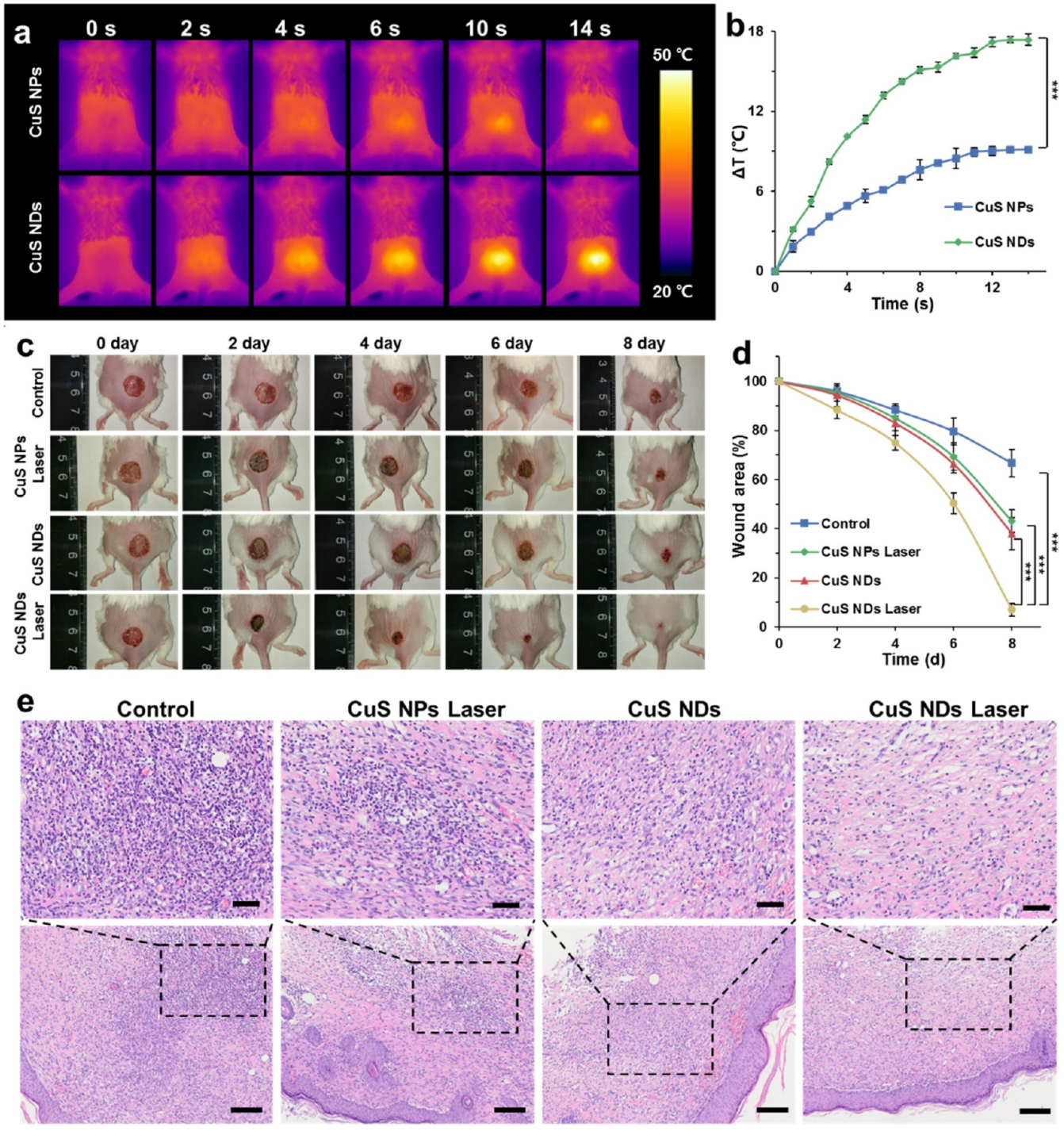

Figure 6. Antibacterial effect of CuS NDs PTT in vivo. (a) Thermal infrared image of temperature evolution on dosed mice upon NIR laser irradiation (45 μg/mL, 2.5 W/cm^2). (b) Temperature evolution profile of dosed mice upon NIR laser irradiation. (c) Wound photographs for different treatment effects of BALB/c mice MRSA-infected wound. (d) Wound area evolution rate of BALB/c mice. (e) Pathologic histological analysis of CuS NDs PTT antibacterial effect. H&E staining of the BALB/c mice dermal wound tissue at day 8 after treatment, up bar = 50 μm, bottom bar = 100 μm.

the generation of ROS occurs upon irradiation. We thus used DCFH-DA to monitor the generation of ROS after different treatments on ESBL *E. coli*. As shown in Figure 4b, the bacteria treated with CuS NPs/CuS NDs with laser treatment present strong fluorescence signal, confirming the ROS generation upon laser irradiation.

Currently, the nanomaterial-mediated antibacterial therapy is involved in different mechanistic aspects to kill bacteria,[39−42] including disruption of bacterial cellular wall/membrane,[43] RNA effluxes,[44] DNA damage,[45] oxidative stress to bacterial cells,[46] and possible inhibition of the bacterial energy metabolism,[47] as well as photothermal antibacterial therapy (involving initiation of sonic and mechanical wave, bubble generation, heat damage, and fusion or disintegration of nanoparticles).[48−50] There are also other results that suggest that the nanoparticles may adhere to the exterior of the cell

DOI: 10.1021/acsami.8b21766
ACS Appl. Mater. Interfaces 2019, 11, 3809−3822

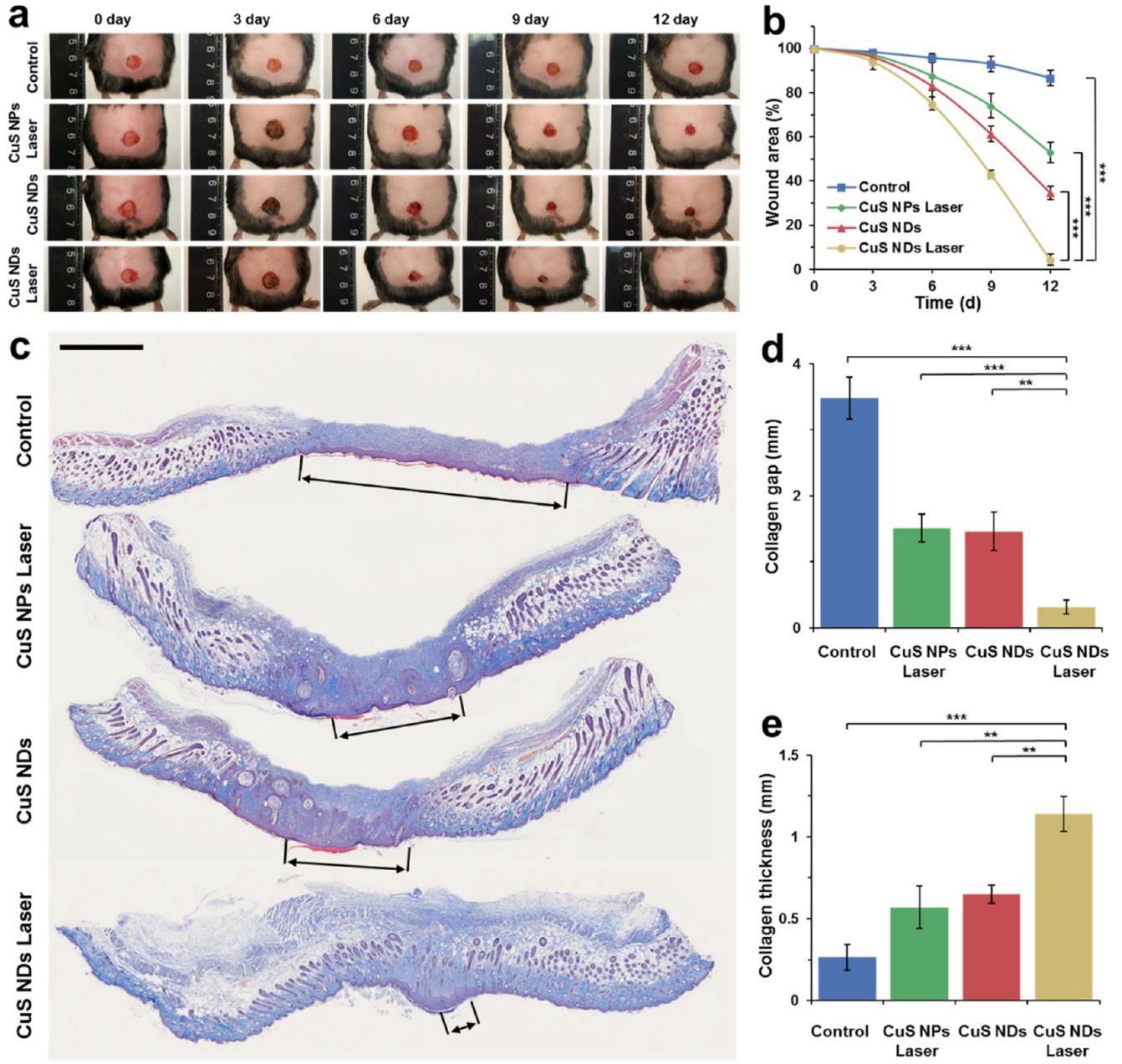

Figure 7. Pathologic histological analysis of CuS NDs PTT promoting healing effect in MRSA-infected diabetic wound model. (a) Digital images of Masson's trichrome-stained (db/db) mice dermal wound tissue at day 12 after wounding and collagen distribution (aquamarine blue) in healed skin as per tissue sections, bar = 1 mm. (b) Quantification of the percentage of wound healing area over time. (c) Vertical section of the wound stained between the euangiotic tissues at both ends and the collagen tissue gap (stained with aquamarine blue) after different treatments. (d) Quantification of the collagen tissue thickness. (e) Quantification of the collagen tissue gap.

wall/membrane, interfering with permeability and negatively influencing the cellular respiratory action and disturbing the metastasis of cells. As for the present study, the treatment of CuS NDs was demonstrated to induce destruction of bacterial cellular wall/membrane integrity and cause variation of the structure. In collaboration with other findings, we propose the antibacterial effect as result of (i) photothermal effects of CuS NDs, (ii) release of Cu^{2+}, and (iii) photodynamic generation of ROS. CuS NDs-mediated phototherapy involves multiple mechanisms of anticancer therapy, and we believe these combinational effects jointly contribute to the efficient antibacterial therapy.

3.6. Promoting Healing Effects of CuS NDs PTT in Vitro. To verify the effect of Cu^{2+} in accelerating the dermal tissue restoration, we chose human foreskin fibroblast cell (HFF-1) for in vitro scratch assay. Following the different treatments of cells scratch, the migration extent displayed a significant difference (Figure 5a). After the treatment with CuS NDs with laser irradiation, the cells exhibited the strongest migration capability. Quantitative analysis results are also in agreement with the migration observation, where the group with CuS NDs with laser irradiation showed the highest migration rate (Figure 5b). Furthermore, we performed the Matrigel assay to simulate the angiogenesis of endothelial cells on top of connective tissue membrane, and human umbilical

DOI: 10.1021/acsami.8b21766
ACS Appl. Mater. Interfaces 2019, 11, 3809−3822

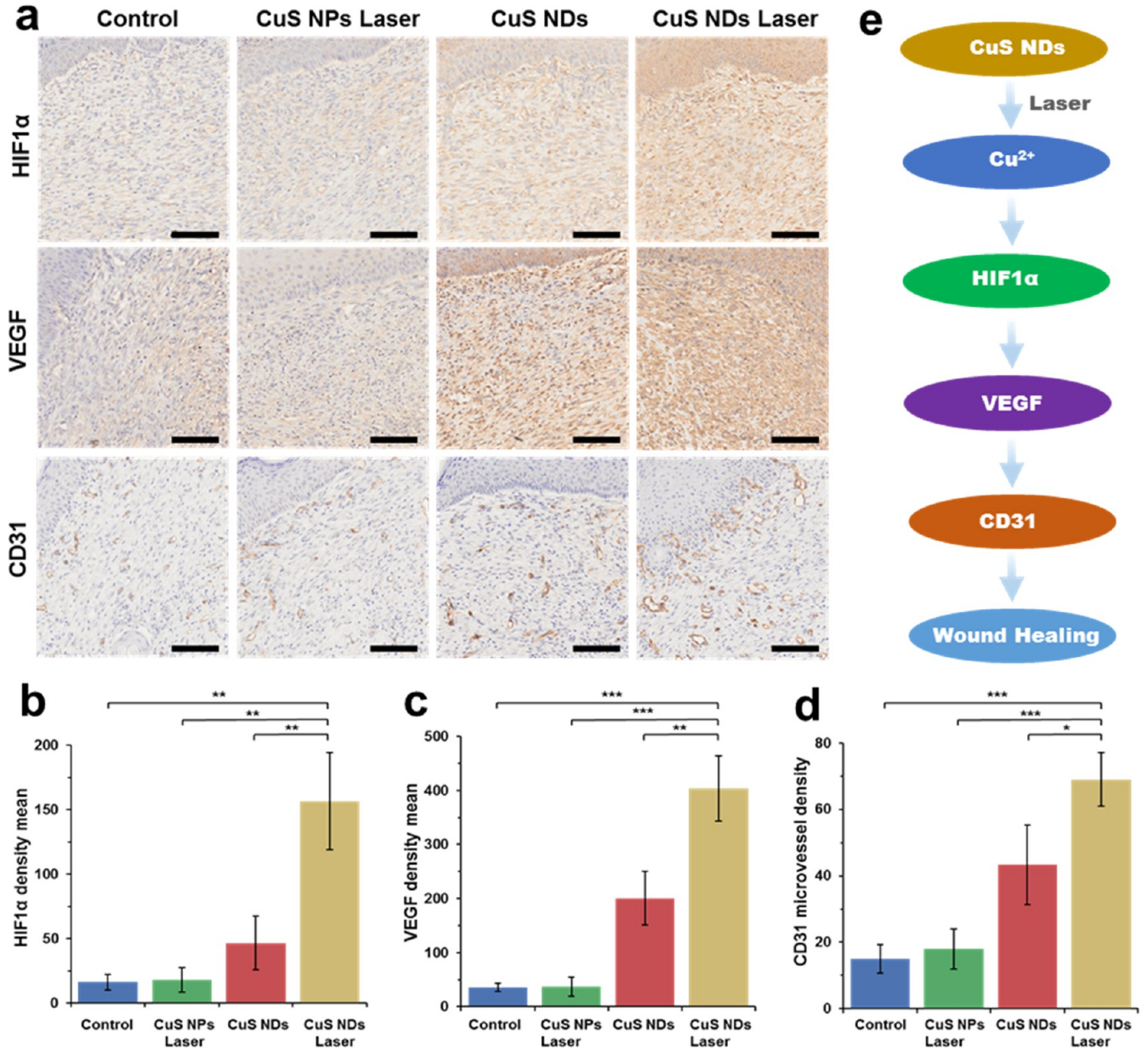

Figure 8. Immunohistochemical staining (a) and quantitative analysis (b–d) of HIF-1α, VEGF, and CD31 in the wound bed on day 12, scale bar = 100 μm. (e) Scheme of possible mechanism.

vein endothelial cells (HUVEC) were used for this assay. As shown in Figure 5c, the cells stretched to form tight junctions, branch nodes, mesh circles, and parallel cell lines, which are the typical indications of the late stage of angiogenesis, after the treatment of CuS NDs with laser irradiation.[46] However, the cells only formed a few short lines and meshes, which were regarded as the early stage of angiogenesis after other treatments. The special HUVEC angiogenesis quantitative analysis of tubule junctions, tubule nodes, and tubule meshes from every group were also in agreement with our observation (Figures 5d and S3a,b).

3.7. Evaluation of in Vivo Antibacterial Effect by BALB/c Wound-Infection Model. To assess the antibacterial effects in vivo, female BALB/c mice with an infected wound on their back were subjected to the indicated treatment. Before the treatment, the ulceration appeared in all treatment groups and remained unhealed even after 6 days (Figure 6). The elevated temperature was observed in the wound area upon laser irradiation of the mice treated with CuS NDs (Figure 6a,b); the highest temperature recorded in the wound area was about 50 °C, which did not lead to the obvious damage to normal tissue. Compared with untreated and other control groups (Figure 6c), the trauma area treated CuS NDs with laser irradiation became much smaller, whereas the treatment of either CuS NDs without laser irradiation, or CuS NPs with laser irradiation, only induced moderate reduction of the trauma area (Figure 6d). As indicated by H&E staining results (Figure 6e), the histological slice of untreated control groups displayed the obvious infiltration of inflammatory cells, which are composed of neutrophils and mononuclear cells adhered to the stratified squamous epithelium. In contrast, the infiltration of inflammatory cells was hardly observed in the mice that were administrated with CuS NDs with laser irradiation. Among all groups, the infiltration degree of inflammatory cells

DOI: 10.1021/acsami.8b21766
ACS Appl. Mater. Interfaces 2019, 11, 3809–3822

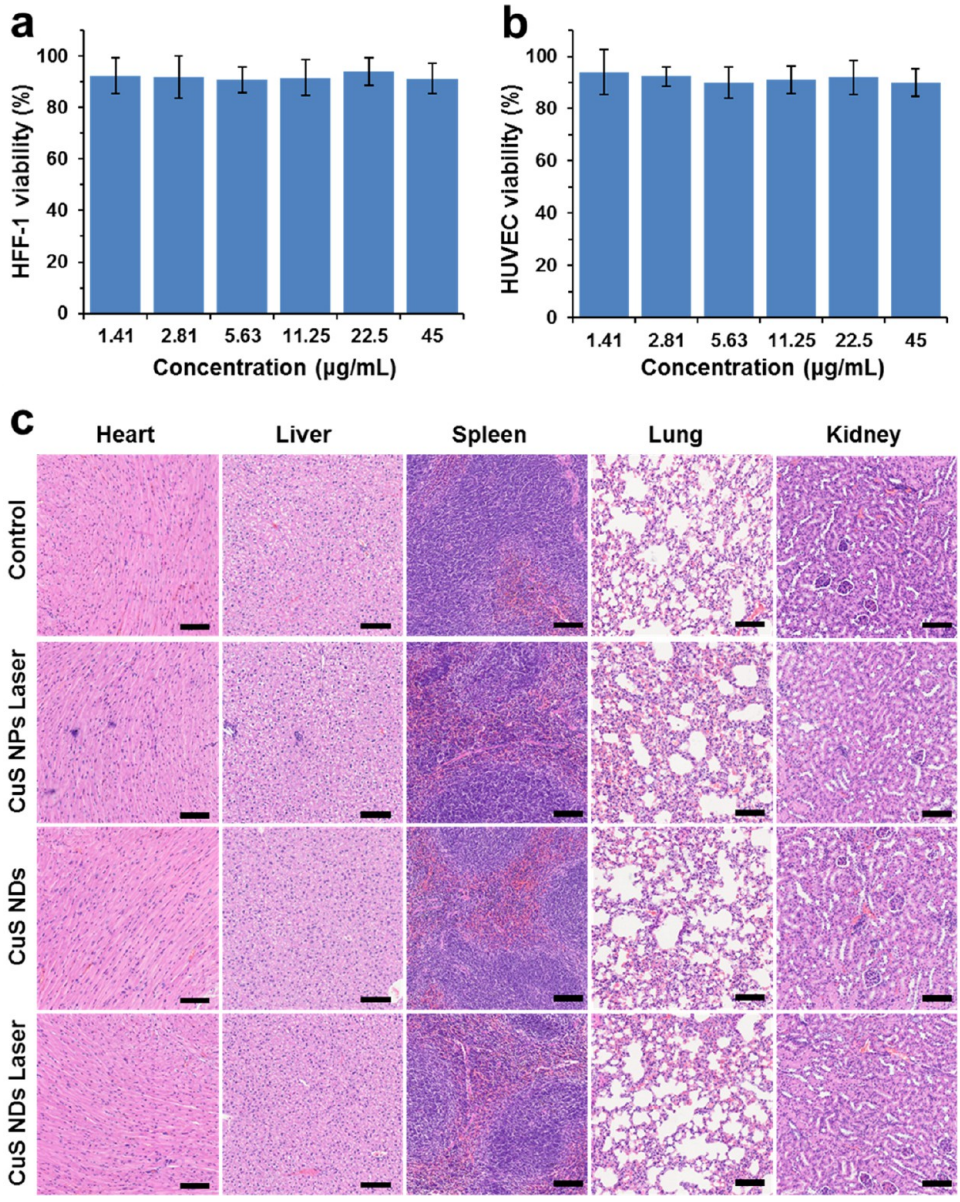

Figure 9. Preliminary toxicity study. Cytotoxicity to (a) HFF-1 and (b) HUVEC with different CuS NDs concentrations with laser irradiation (2.5 W/cm^2, 10 min). (c) Histological toxicological observation of H&E staining of tissues of major organs (heart, liver, spleen, lung, and kidney; bar = 100 μm).

from either CuS NDs, or the CuS NPs laser group, is moderate, suggesting their weak antibacterial effects. These results demonstrated the effectiveness of irradiation-mediated photothermal treatment to reduce the burden of bacterial infection in vivo.

3.8. Promoting Healing Effects and Potential Mechanism of CuS NDs PTT in Vivo. As typical chronic nonhealing wounds, chronic diabetes wounds remain a major challenge for treatment in clinic. The bacteria-infected dermal wound model in diabetic mice was used to evaluate the antibacterial effects and wound-healing effects of our samples owing to its validated, reproducible, and readily available characteristics.[51,52] We further evaluated whether the treatment modality we have developed could promote tissue restoration. To this end, diabetic mutant (db/db) mice with MRSA-infected wounds were established as the drug-resistant infected chronic nonhealing wound model for in vivo study. The wounds of mice treated with CuS NDs with laser irradiation almost disappeared completely at day 12, whereas other indicated treatments induced incomplete recovery (Figure 7a,b).

We further performed the Masson's trichrome (MT) staining to analyze the histological characteristics of in vivo promoting healing effects in terms of collagen gap and thickness. The vertical section was stained between the euangiotic tissues at both ends, and the collagen tissue gap (stained with aquamarine blue) after different treatments was observed (Figure 7c). The shortest gap was observed with CuS NDs treatment with laser irradiation, whereas the largest gap and thickest euangiotic tissue were observed in the control group (Figure 7d,e).

Local wound hypoxia plays an important role in determining the success of the healing process.[9−12] As the main regulator of oxygen homeostasis, hypoxia-inducible factor-1 (HIF-1) is an important determinant of healing effect. The presence of HIF-1α was almost negligible in control and CuS NPs laser groups,

DOI: 10.1021/acsami.8b21766
ACS Appl. Mater. Interfaces 2019, 11, 3809−3822

indicating their low expression (Figure 8a,b). The CuS NDs demonstrated a higher HIF-1α expression. However, HIF-1α was upregulated in the wound bed area in the CuS NDs laser groups owing to the obvious simulation of HIF-1α protein concentration. VEGF, as a direct neovascularization important factor for wound healing, was also upregulated in the wound area (Figure 8a,c). A significant improvement in the total number of vessels was investigated by staining with an anti-CD31 antibody in the CuS NDs laser groups compared with the other groups (Figure 8a,d). The possible mechanism of the CuS NDs laser-mediated wound healing is shown in Figure 8e. The release of copper ion could be controlled by CuS NDs under laser irradiation, and the released Cu^{2+} may upregulate HIF-1α. High expression of HIF-1α induced higher concentration of angiogenesis relative cells and formation of more vessels in the core position of skin formation process, and finally improved the local wound healing.

3.9. Pilot Toxicity Study. To evaluate the potential toxicity of CuS NDs after the laser irradiation, in vitro cytotoxicity experiments were operated with 2 human skin cell lines, namely, HFF-1 cells and HUVECs. As shown in Figure 9a,b, cell viability was independent of dose of the CuS NDs with laser irradiation, and both cell lines were still viable even at the concentration of 45 μg/mL, indicating the low cytotoxic nature of CuS NDs and photocytotoxicity. The toxicity to major organs was further investigated by H&E staining (Figure 9c). H&E indicated that CuS NDs with laser irradiation did not show any significant histological changes or toxicity within the treatment period, and there was no death or significant weight loss in in vivo experimental results, suggesting its safety and good biocompatibility in vivo. Furthermore, the body weight remained steady after the treatment (Figure S4a). In the meantime, the liver function index (such as ALT and AST) and kidney function index through blood biochemistry test (Figure S4b) remain almost unchanged after the treatment of CuS NDs with laser irradiation. All these results strongly demonstrate that our developed therapeutic strategy is safe for in vivo application of antibacterial therapy and wound healing.

4. CONCLUSIONS

In summary, we developed a new class of nanomedicine as an effective strategy for the treatment of chronic nonhealing infectious wounds. This strategy relies on both photothermal and photodynamic effects of CuS to eradicate bacteria and the released Cu^{2+} to accelerate wound-healing process by promoting the angiogenesis of endothelial cells in the wound area. As a result, the formulation of CuS ND could effectively treat bacteria-infected chronic nonhealing wounds under laser irradiation. We demonstrated that such a therapeutic modality was effective in inhibiting drug-resistant pathogens, including MRSA and ESBL *E. coli* both in vitro and in vivo, and in curing infectious wounds in vivo with negligible local or systemic toxicities. Our strategy offers an effective antibacterial therapeutic modality for the treatment of chronic infectious wounds in the dawning era of precision medicine.

ASSOCIATED CONTENT

Supporting Information

The Supporting Information is available free of charge on the ACS Publications website at DOI: 10.1021/acsami.8b21766.

Materials, experimental methods, ROS analysis, SEM analysis, and endothelial tubulogenesis analysis (PDF)

AUTHOR INFORMATION

Corresponding Authors

*E-mail: helder.santos@helsinki.fi (H.A.S.).
*E-mail: zhoum@zju.edu.cn (M.Z.).

ORCID

Hélder A. Santos: 0000-0001-7850-6309
Min Zhou: 0000-0002-7319-9570

Author Contributions

⋈Y.Q., Y.P., and H.Z. contributed equally to this work.

Notes

The authors declare no competing financial interest.

ACKNOWLEDGMENTS

This work was supported by the National Key R&D Program of China (2018YFC0115701) and the National Natural Science Foundation of China (No. 81671748). Prof. H. Zhang acknowledges Jane and Aatos Erkko Foundation (Grant no. 4704010), Academic of Finland (Grant no. 297580) and Sigrid Juselius Foundation (Grant no. 28001830K1) for financial support. Prof. H. A. Santos acknowledges financial support from the Sigrid Jusélius Foundation (Decision no. 4704580) and the Helsinki Institute of Life Science Funds.

REFERENCES

(1) Cavanagh, P. R.; Lipsky, B. A.; Bradbury, A. W.; Botek, G. Treatment for Diabetic Foot Ulcers. *Lancet* **2005**, *366*, 1725−1735.

(2) Kanter, J. E.; Kramer, F.; Barnhart, S.; Averill, M. M.; Vivekanandan-Giri, A.; Vickery, T.; Li, L. O.; Becker, L.; Yuan, W.; Chait, A.; Braun, K. R.; Potter-Perigo, S.; Sanda, S.; Wight, T. N.; Pennathur, S.; Serhan, C. N.; Heinecke, J. W.; Coleman, R. A.; Bornfeldt, K. E. Diabetes Promotes an Inflammatory Macrophage Phenotype and Atherosclerosis Through Acyl-CoA Synthetase 1. *Proc. Natl. Acad. Sci. U.S.A.* **2012**, *109*, E715−E724.

(3) Falanga, V. Wound Healing and its Impairment in the Diabetic Foot. *Lancet* **2005**, *366*, 1736−1743.

(4) Guo, S.; DiPietro, L. A. Factors Affecting Wound Healing. *J. Dent. Res.* **2010**, *89*, 219−229.

(5) Lipsky, B. A.; Berendt, A. R.; Cornia, P. B.; Pile, J. C.; Peters, E. J. G.; Armstrong, D. G.; Deery, H. G.; Embil, J. M.; Joseph, W. S.; Karchmer, A. W.; Pinzur, M. S.; Senneville, E. 2012 Infectious Diseases Society of America Clinical Practice Guideline for the Diagnosis and Treatment of Diabetic Foot Infections. *Clin. Infect. Dis.* **2012**, *54*, E132−U232.

(6) Bjarnsholt, T.; Kirketerp-Moller, K.; Jensen, P. O.; Madsen, K. G.; Phipps, R.; Krogfelt, K.; Hoiby, N.; Givskov, M. Why Chronic Wounds will not Heal: A Novel Hypothesis. *Wound Repair Regener.* **2008**, *16*, 2−10.

(7) James, G. A.; Swogger, E.; Wolcott, R.; Pulcini, Ed; Secor, P.; Sestrich, J.; Costerton, J. W.; Stewart, P. S. Biofilms in Chronic Wounds. *Wound Repair Regener.* **2008**, *16*, 37−44.

(8) Sanchez, C. J., Jr.; Mende, K.; Beckius, M. L.; Akers, K. S.; Romano, D. R.; Wenke, J. C.; Murray, C. K. Biofilm Formation by Clinical Isolates and the Implications in Chronic Infections. *BMC Infect. Dis.* **2013**, *13*, No. 47.

(9) Kornblatt, A. P.; Nicoletti, V. G.; Travaglia, A. The Neglected Role of Copper Ions in Wound Healing. *J. Inorg. Biochem.* **2016**, *161*, 1−8.

(10) Zhang, Z.; Qiu, L. Y.; Lin, C.; Yang, H.; Fu, H. Y.; Lia, R.; Kang, Y. J. Copper-Dependent and -Independent Hypoxia-Inducible Factor-1 Regulation of Gene Expression. *Metallomics* **2014**, *6*, 1889−1893.

(11) Zimnicka, A. M.; Tang, H. Y.; Guo, Q.; Kuhr, F. K.; Oh, M. J.; Wan, J.; Chen, J. W.; Smith, K. A.; Fraidenburg, D. R.; Choudhury, M. S. R.; Levitan, I.; Machado, R. F.; Kaplan, J. H.; Yuan, J. X. J.

DOI: 10.1021/acsami.8b21766
ACS Appl. Mater. Interfaces 2019, 11, 3809−3822

Upregulated Copper Transporters in Hypoxia-Induced Pulmonary Hypertension. *PLoS One* **2014**, *9*, No. e90544.
(12) Himoto, T.; Fujita, K.; Nomura, T.; Tani, J.; Miyoshi, H.; Morishita, A.; Yoneyama, H.; Kubota, S.; Haba, R.; Suzuki, Y.; Masaki, T. Roles of Copper in Hepatocarcinogenesis via the Activation of Hypoxia-Inducible Factor-1 alpha. *Biol. Trace Elem. Res.* **2016**, *174*, 58−64.
(13) Wu, C.; Zhou, Y.; Xu, M.; Han, P.; Chen, L.; Chang, J.; Xiao, Y. Copper-Containing Mesoporous Bioactive Glass Scaffolds with Multifunctional Properties of Angiogenesis Capacity, Osteostimulation and Antibacterial Activity. *Biomaterials* **2013**, *34*, 422−433.
(14) Zhao, S. C.; Wang, H.; Zhang, Y. D.; Huang, W. H.; Rahaman, M. N.; Liu, Z. T.; Wang, D. P.; Zhang, C. Q. Copper-Doped Borosilicate Bioactive Glass Scaffolds with Improved Angiogenic and Osteogenic Capacity for Repairing Osseous Defectse. *Acta Biomater.* **2015**, *14*, 185−196.
(15) Yu, Q.; Han, Y.; Wang, X.; Qin, C.; Zhai, D.; Yi, Z.; Chang, J.; Xiao, Y.; Wu, C. Copper Silicate Hollow Microspheres-Incorporated Scaffolds for Chemo-Photothermal Therapy of Melanoma and Tissue Healing. *ACS Nano* **2018**, *12*, 2695−2707.
(16) Zhao, S.; Li, L.; Wang, H.; Zhang, Y.; Cheng, X.; Zhou, N.; Rahaman, M. N.; Liu, Z.; Huang, W.; Zhang, C. Wound Dressings Composed of Copper-Doped Borate Bioactive Glass Microfibers Stimulate Angiogenesis and Heal Full-Thickness Skin Defects in a Rodent Model. *Biomaterials* **2015**, *53*, 379−391.
(17) Bari, A.; Bloise, N.; Fiorilli, S.; Novajra, G.; Vallet-Regi, M.; Bruni, G.; Torres-Pardo, A.; Gonzalez-Calbet, J. M.; Visai, L.; Vitale-Brovarone, C. Copper-Containing Mesoporous Bioactive Glass Nanoparticles as Multifunctional Agent for Bone Regeneration. *Acta Biomater.* **2016**, *55*, 493−504.
(18) Hu, D.; Li, H.; Wang, B.; Ye, Z.; Lei, W.; Jia, F.; Jin, Q.; Ren, K.-F.; Ji, J. Surface-Adaptive Gold Nanoparticles with Effective Adherence and Enhanced Photothermal Ablation of Methicillin-Resistant *Staphylococcus aureus* Biofilm. *ACS Nano* **2017**, *11*, 9330−9339.
(19) Wu, M.-C.; Deokar, A. R.; Liao, J.-H.; Shih, P.-Y.; Ling, Y.-C. Graphene-Based Photothermal Agent for Rapid and Effective Killing of Bacteria. *ACS Nano* **2013**, *7*, 1281−1290.
(20) Qian, W.; Yan, C.; He, D.; Yu, X.; Yuan, L.; Liu, M.; Luo, G.; Deng, J. pH-Triggered Charge-Reversible of Glycol Chitosan Conjugated Carboxyl Graphene for Enhancing Photothermal Ablation of Focal Infection. *Acta Biomater.* **2018**, *15*, 256−264.
(21) Wang, B.; Feng, G.; Seifrid, M.; Wang, M.; Liu, B.; Bazan, G. C. Antibacterial Narrow-Band-Gap Conjugated Oligoelectrolytes with High Photothermal Conversion Efficiency. *Angew. Chem., Int. Ed.* **2017**, *56*, 16063−16066.
(22) Jin, Y.; Deng, J.; Yu, J.; Yang, C.; Tong, M.; Hou, Y. Fe_5C_2 Nanoparticles: A Reusable Bactericidal Material with Photothermal Effects Under Near-Infrared Irradiation. *J. Mater. Chem. B* **2015**, *3*, 3993−4000.
(23) Fasciani, C.; Jazmin Silvero, M.; Alexandra Anghel, M.; Argueello, G. A.; Cecilia Becerra, M.; Scaiano, J. C. Aspartame-Stabilized Gold-Silver Bimetallic Biocompatible Nanostructures with Plasmonic Photothermal Properties, Antibacterial Activity, and Long-Term Stability. *J. Am. Chem. Soc.* **2014**, *136*, 17394−17397.
(24) Kim, J.-W.; Shashkov, E. V.; Galanzha, E. I.; Kotagiri, N.; Zharov, V. P. Photothermal Antimicrobial Nanotherapy and Nanodiagnostics with Self-Assembling Carbon Nanotube Clusters. *Lasers Surg. Med.* **2007**, *39*, 622−634.
(25) Huang, W.-C.; Tsai, P.-J.; Chen, Y.-C. Multifunctional Fe_3O_4@Au Nanoeggs as Photothermal Agents for Selective Killing of Nosocomial and Antibiotic-Resistant Bacteria. *Small* **2009**, *5*, 51−56.
(26) Zhou, M.; Li, J.; Liang, S.; Sood, A. K.; Liang, D.; Li, C. CuS Nanodots with Ultrahigh Efficient Renal Clearance for Positron Emission Tomography Imaging and Image-Guided Photothermal Therapy. *ACS Nano* **2015**, *9*, 7085−7096.
(27) Zhou, M.; Ku, G.; Pageon, L.; Li, C. Theranostic Probe for Simultaneous in Vivo Photoacoustic Imaging and Confined Photothermolysis by Pulsed Laser At 1064 Nm In 4T1 Breast Cancer Model. *Nanoscale* **2014**, *6*, 15228−15235.
(28) Zhou, M.; Zhang, R.; Huang, M.; Lu, W.; Song, S.; Melancon, M. P.; Tian, M.; Liang, D.; Li, C. A Chelator-Free Multifunctional [^{64}Cu]Cus Nanoparticle Platform for Simultaneous Micro-PET/CT Imaging and Photothermal Ablation Therapy. *J. Am. Chem. Soc.* **2010**, *132*, 15351−15358.
(29) Wang, S. H.; Riedinger, A.; Li, H. B.; Fu, C. H.; Liu, H. Y.; Li, L. L.; Liu, T. L.; Tan, L. F.; Barthel, M. J.; Pugliese, G.; De Donato, F.; D'Abbusco, M. S.; Meng, X. W.; Manna, L.; Meng, H.; Pellegrino, T. Plasmonic Copper Sulfide Nanocrystals Exhibiting Near-Infrared Photothermal and Photodynamic Therapeutic Effects. *ACS Nano* **2015**, *9*, 1788−1800.
(30) Li, B.; Wang, Q.; Zou, R. J.; Liu, X. J.; Xu, K. B.; Li, W. Y.; Hu, J. Q. $Cu_{7.2}S_4$ Nanocrystals: a Novel Photothermal Agent with a 56.7% Photothermal Conversion Efficiency for Photothermal Therapy of Cancer Cells. *Nanoscale* **2014**, *6*, 3274−3282.
(31) Ramadan, S.; Guo, L. R.; Li, Y. J.; Yan, B. F.; Lu, W. Hollow Copper Sulfide Nanoparticle-Mediated Transdermal Drug Delivery. *Small* **2012**, *8*, 3143−3150.
(32) Zhao, Y.; Cai, Q.; Qi, W.; Jia, Y.; Xiong, T.; Fan, Z.; Liu, S.; Yang, J.; Chang, B.; et al. BSA-CuS Nanoparticles for Photothermal Therapy of Diabetic Wound Infection in Vivo. *ChemistrySelect* **2018**, *3*, 9510−9516.
(33) Dai, X.; Zhao, Y.; Yu, Y.; Chen, X.; Wei, X.; Zhang, X.; Li, C. Single Continuous Near-Infrared Laser-Triggered Photodynamic and Photothermal Ablation of Antibiotic-Resistant Bacteria Using Effective Targeted Copper Sulfide Nanoclusters. *ACS Appl. Mater. Interfaces* **2017**, *9*, 30470−30479.
(34) Huang, J.; Zhou, J.; Zhuang, J.; Gao, H.; Huang, D.; Wang, L.; Wu, W.; Li, Q.; Yang, D.-P.; Han, M.-Y. Strong Near-Infrared Absorbing and Biocompatible CuS Nanoparticles for Rapid and Efficient Photothermal Ablation of Gram-Positive and -Negative Bacteria. *ACS Appl. Mater. Interfaces* **2017**, *9*, 36606−36614.
(35) Wang, H.-Y.; Hua, X.-W.; Wu, F.-G.; Li, B.; Liu, P.; Gu, N.; Wang, Z.; Chen, Z. Synthesis of Ultrastable Copper Sulfide Nanoclusters via Trapping the Reaction Intermediate: Potential Anticancer and Antibacterial Applications. *ACS Appl. Mater. Interfaces* **2015**, *7*, 7082−7092.
(36) Hu, X.; Li, L.; Lu, Y.; Liu, C.; Lei, Y.; Zhang, C.; Yin, Q.; Zhang, Y. Multifunctional CuS Nanocrystals for Inhibiting Both Osteosarcoma Proliferation and Bacterial Infection by Photothermal Therapy. *J. Nanoparticle Res.* **2017**, *19*, No. 295.
(37) Li, L. H.; Rashidi, L. H.; Yao, M. Y.; Ma, L.; Chen, L. L.; Zhang, J. Y.; Zhang, Y.; Chen, W. CuS Nanoagents for Photodynamic and Photothermal Therapies: Phenomena and Possible Mechanisms. *Photodiagn. Photodyn. Ther.* **2017**, *19*, 5−14.
(38) Lu, Y.; Li, L.; Lin, Z.; Wang, L.; Lin, L.; Li, M.; Zhang, Y.; Yin, Q.; Li, Q.; Xia, H. A New Treatment Modality for Rheumatoid Arthritis: Combined Photothermal and Photodynamic Therapy Using $Cu_{7.2}S_4$ Nanoparticles. *Adv. Healthcare Mater.* **2018**, *7*, No. 1800013.
(39) Naraginti, S.; Sivakumar, A. Eco-Friendly Synthesis of Silver and Gold Nanoparticles with Enhanced Bactericidal Activity and Study of Silver Catalyzed Reduction of 4-Nitrophenol. *Spectrochim. Acta, Part A* **2014**, *128*, 357−362.
(40) Salunke, G. R.; Ghosh, S.; Santosh Kumar, R. J.; Khade, S.; Vashisth, P.; Kale, T.; Chopade, S.; Pruthi, V.; Kundu, G.; Bellare, J. R.; Chopade, B. A. Rapid Efficient Synthesis and Characterization of Silver, Gold, and Bimetallic Nanoparticles From the Medicinal Plant *Plumbago zeylanica* and Their Application in Biofilm Control. *Int. J. Nanomed.* **2014**, *9*, 2635−2653.
(41) Shrivastava, S.; Bera, T.; Singh, S. K.; Singh, G.; Ramachandrarao, P.; Dash, D. Characterization of Antiplatelet Properties of Silver Nanoparticles. *ACS Nano* **2009**, *3*, 1357−1364.
(42) Tamayo, L. A.; Zapata, P. A.; Vejar, N. D.; Azocar, M. I.; Gulppi, M. A.; Zhou, X.; Thompson, G. E.; Rabagliati, F. M.; Paez, M. A. Release of Silver and Copper Nanoparticles From Polyethylene Nanocomposites and Their Penetration Into Listeria Monocytogenes. *Mater. Sci. Eng., C* **2014**, *40*, 24−31.

DOI: 10.1021/acsami.8b21766
ACS Appl. Mater. Interfaces 2019, 11, 3809−3822

(43) Tang, J.; Chen, Q.; Xu, L.; Zhang, S.; Feng, L.; Cheng, L.; Xu, H.; Liu, Z.; Peng, R. Graphene Oxide−Silver Nanocomposite As a Highly Effective Antibacterial Agent with Species-Specific Mechanisms. *ACS Appl. Mater. Interfaces* **2013**, *5*, 3867−3874.
(44) Akhavan, O.; Ghaderi, E. Toxicity of Graphene and Graphene Oxide Nanowalls Against Bacteria. *ACS Nano* **2010**, *4*, 5731−5736.
(45) Nel, A.; Xia, T.; Mädler, L.; Li, N. Toxic Potential of Materials at the Nanolevel. *Science* **2006**, *311*, 622−627.
(46) Kang, S.; Herzberg, M.; Rodrigues, D. F.; Elimelech, M. Antibacterial Effects of Carbon Nanotubes: Size Does Matter! *Langmuir* **2008**, *24*, 6409−6413.
(47) Mashino, T.; Okuda, K.; Hirota, T.; Hirobe, M.; Nagano, T.; Mochizuki, M. Inhibition of *E. coli* Growth by Fullerene Derivatives and Inhibition Mechanism. *Bioorg. Med. Chem. Lett.* **1999**, *9*, 2959−2962.
(48) Wang, S.; Singh, A. K.; Senapati, D.; Neely, A.; Yu, H.; Ray, P. C. Rapid Colorimetric Identification and Targeted Photothermal Lysis of Salmonella Bacteria by Using Bioconjugated Oval-Shaped Gold Nanoparticles. *Chem. - Eur. J.* **2010**, *16*, 5600−5606.
(49) Zharov, V. P.; Mercer, K. E.; Galitovskaya, E. N.; Smeltzer, M. S. Photothermal Nanotherapeutics and Nanodiagnostics for Selective Killing of Bacteria Targeted with Gold Nanoparticles. *Biophys. J.* **2006**, *90*, 619−627.
(50) Letfullin, R. R.; Joenathan, C.; George, T. F.; Zharov, V. P. Laser-Induced Explosion of Gold Nanoparticles: Potential Role For Nanophotothermolysis of Cancer. *Nanomedicine* **2006**, *1*, 473−480.
(51) Xiao, J.; Chen, S.; Yi, J.; Zhang, H. F.; Ameer, G. A Cooperative Copper Metal−Organic Framework-Hydrogel System Improves Wound Healing in Diabetes. *Adv. Funct. Mater.* **2017**, *12*, No. 1604872.
(52) Xiao, J.; Zhu, Y.; Huddleston, S.; Li, P.; Xiao, B.; Farha, O.; Ameer, G. A Copper Metal−Organic Framework Nanoparticles Stabilized with Folic Acid Improve Wound Healing in Diabetes. *ACS Nano* **2018**, *12*, 1023−1032.

DOI: 10.1021/acsami.8b21766
ACS Appl. Mater. Interfaces 2019, 11, 3809−3822